ARTICLE

Neural mechanisms underlying reduced nocifensive sensitivity in autism-associated *Shank3* mutant dogs

Qi Shi[1,2], Baolong Ren[1,2], Xuejing Lu[3,4], Libo Zhang[3,4], Liang Wu[1], Li Hu[3,4]✉ and Yong Q. Zhang[1,5]✉

Autistic individuals carrying mutations in *SHANK3* (encoding a synaptic scaffolding protein) have been consistently reported to exhibit reduced pain sensitivity. However, the neural mechanisms underlying impaired pain processing remain unclear. To investigate the role of *SHANK3* in pain processing, we conducted behavioral, electrophysiological, and pharmacological tests upon nociceptive stimulation in a *Shank3* mutant dog model. Behaviorally, *Shank3* mutant dogs showed reduced nocifensive sensitivity compared to wild-type (WT) dogs. Electrophysiologically, *Shank3* mutant dogs exhibited reduced neural responses elicited by the activations of both Aδ- and C-fiber nociceptors. Additionally, *Shank3* mutants showed a lower level of aperiodic exponents, which serve as a marker for the excitatory-inhibitory balance of neural activity. The aperiodic exponents mediated the relationship between genotype and nocifensive sensitivity as well as between genotype and neural responses elicited by nociceptive stimuli. Pharmacologically, the reduced nocifensive sensitivity and atypical excitatory-inhibitory balance were rescued by a $GABA_AR$ antagonist pentylenetetrazole. These findings highlight the critical role of *Shank3* in pain processing and suggest that an impaired excitatory-inhibitory balance may be responsible for the reduced nocifensive reactivity in autism.

Molecular Psychiatry; https://doi.org/10.1038/s41380-025-02952-y

INTRODUCTION

Pain is essential for alerting individuals to potential dangers and facilitating self-protection [1]. Abnormal pain perception can lead to unnecessary suffering or increased risks of harm. In individuals with autism, altered pain perception has been linked to a significantly heightened risk of injury-related death [2]. Many autistic individuals exhibit hyposensitivity to pain [3, 4] and often engage in self-injurious behaviors [5]. Consistently, neurophysiological studies reveal reduced responses to nociceptive stimuli in autistic individuals, providing objective evidence of altered pain processing [6, 7].

Several genes have been implicated in altered pain processing in autism, including *SCN9A* [8] and *SHANK3* [9]. *SHANK3* is a high profile autism-related gene, with mutations found in over 1% of autism cases [10, 11]. Autistic individuals carrying *SHANK3* mutations exhibit higher pain thresholds compared to typically developing peers and other autistic individuals [12, 13]. However, the neural mechanisms underlying this reduced pain sensitivity due to *SHANK3* mutations remain largely unexplored.

Animal models have been used to investigate the neural mechanisms of altered pain sensitivity in autism. Reduced behavioral sensitivities to various nociceptive stimuli, including mechanical, thermal, inflammatory, and neuropathic, have been observed in rodent [14–16] and monkey [17] models of autism. For instance, $Shank3^{\Delta ex4-22}$ mutant mice exhibited reduced heat hyperalgesia, potentially linked to disrupted expression of the transient receptor potential subtype V1, which regulates heat transduction and interacts with SHANK3 in dorsal root ganglion neurons [18].

Unlike other animal models, dogs have been domesticated for over 30,000 years and share various emotional and cognitive traits with humans [19, 20]. Additionally, the somatosensory system including components of the peripheral and central nervous systems in domestic dogs closely resembles that of humans [21, 22]. Moreover, there are strong parallels in behavioral responses and neurophysiological processes to pain between humans and dogs [23, 24]. These features make dogs an ideal model for studying autism and offer the potentials to provide valuable insights into the neural mechanisms underlying altered pain sensitivity in autism.

Spontaneous electrophysiological activities in the brain are composed of both oscillatory activities and background aperiodic components. Oscillatory activities are periodic and exhibit frequency-specific "narrowband" power, appearing as peaks in the power spectrum. Aperiodic activities are distributed across multiple frequency bands, typically exhibiting a 1/f power distribution [25, 26]. The slope of the aperiodic signal (i.e., the aperiodic exponent) is regarded as a marker for the excitatory-inhibitory (E/I) balance of neural activity [27], which is crucial for nociceptive processing [28–31]. Notably, the relationship between the aperiodic exponent and E/I balance is supported by computational models [32–34] and empirical findings [33, 35]. Targeting GABA signaling could modulate the aperiodic

[1]State Key Laboratory of Molecular Developmental Biology, Institute of Genetics and Developmental Biology, Chinese Academy of Sciences, Beijing 100101, China. [2]University of Chinese Academy of Sciences, Beijing 100101, China. [3]State Key Laboratory of Cognitive Science and Mental Health, Institute of Psychology, Chinese Academy of Sciences, Beijing 100101, China. [4]Department of Psychology, University of Chinese Academy of Sciences, Beijing 100049, China. [5]School of Life Sciences, Hubei University, Wuhan 430415, China. ✉email: huli@psych.ac.cn; yqzhang@genetics.ac.cn

Received: 15 November 2024 Revised: 15 February 2025 Accepted: 10 March 2025
Published online: 17 March 2025

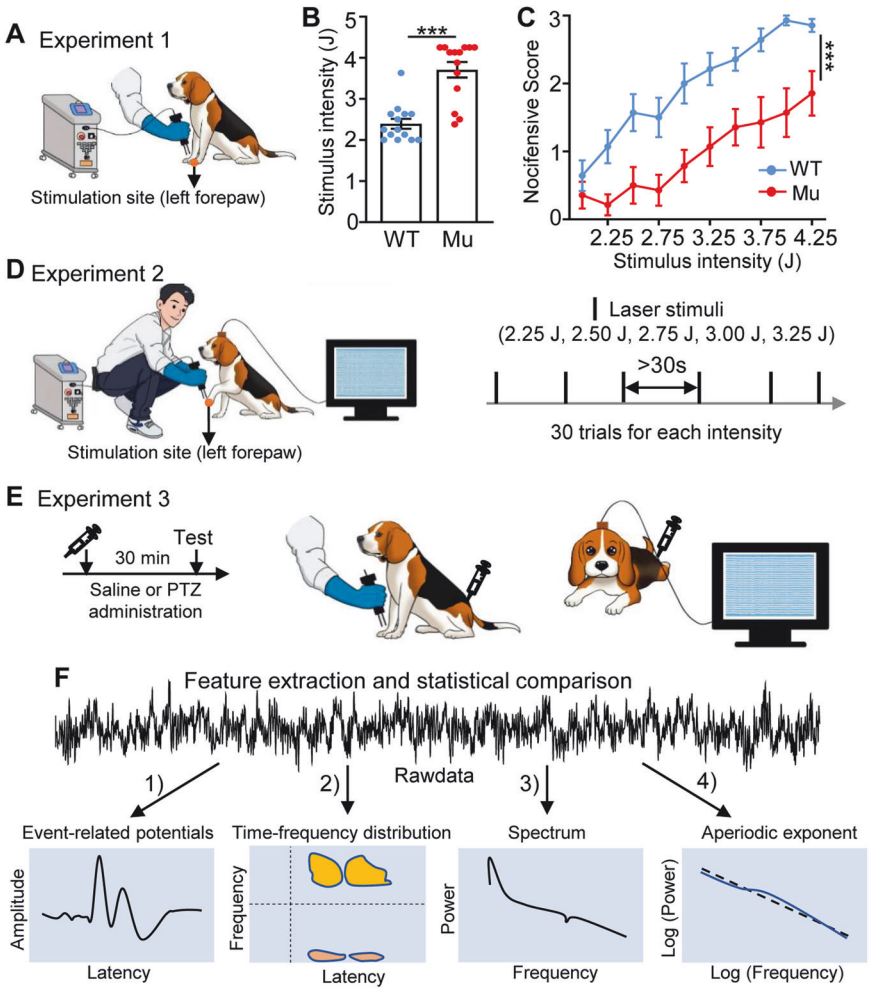

Fig. 1 Experimental design and behavioral results. A Schematic of the nocifensive sensitivity test in dogs (Experiment 1). Laser stimuli were delivered to the skin of the shaved left forepaw (indicated in orange). **B** Comparison of the nocifensive threshold between *Shank3* mutant (Mu, $N = 14$) and wild-type (WT, $N = 14$) dogs. Data are presented as mean ± SEM, with statistical significance determined using the Mann-Whitney *U* test, $^{***}p < 0.001$. **C** Comparisons of nocifensive behavior scores between *Shank3* mutant and WT dogs at different stimulus intensities. Data are presented as mean ± SEM. Statistical significance was determined using two-way repeated-measures ANOVA. $N = 14$ for each condition of each group. $^{***}p < 0.001$. **D** Schematic of the recording of the laser evoked potentials (Experiment 2), which involved five stimulus intensities and 30 trials for each intensity. The inter-stimulus interval was more than 30 s. **E** Schematic depicting the nocifensive sensitivity test and electrophysiological signal recording after saline or pentylenetetrazole (PTZ) administration. **F** The analyses of electrophysiological signals included: 1) event-related potentials, 2) time-frequency distributions, 3) spectral analysis, and 4) aperiodic exponent analysis.

component [36] and the E/I balance to normalize nociceptive sensitivity in chronic neuropathic pain mice [37].

To reveal the neural mechanisms of impaired nocifensive processing due to *Shank3* mutations, we conducted behavioral, electrophysiological, and pharmacological rescue tests upon nociceptive stimulation using a previous established *Shank3* mutant dog model (Fig. 1), which exhibited social and sensory impairments associated with autism [38, 39]. First, we assessed whether *Shank3* mutant dogs exhibited reduced nocifensive sensitivity similar to that observed in autistic individuals and rodent models (Experiment 1). We then evaluated cortical responses to nociceptive stimuli in both time and time-frequency domains to better understand the behavioral phenotypes (Experiment 2). Next, we investigated the potential neural mechanisms underlying the reduced nocifensive sensitivity in *Shank3* mutant dogs, focusing on resting-state brain oscillations and particularly the aperiodic exponent, which serves as a marker for the excitatory-inhibitory balance of neural activity [33]. Finally, we examined whether a $GABA_A$ receptor ($GABA_AR$) antagonist, i.e., pentylenetetrazole (PTZ), could rescue the abnormal nocifensive sensitivity (Experiment 3), as this drug may correct the atypical excitatory-inhibitory balance by increasing resting-state brain oscillations [40]. The findings from the present study provide mechanistic insights into the abnormal nocifensive processing in individuals with autism, and may suggest potential targets for developing interventions for autism.

MATERIALS AND METHODS

Ethics approval and consent to participate

All animal care, surgical and experimental procedures in this study strictly adhered to the guidelines for animal experimentation and were approved by the ethics committee of the Institute of Genetics and Developmental Biology, Chinese Academy of Sciences (AP2022033 and AP2024026).

Animal husbandry

All dogs were housed individually in home cages ($1 \times 1 \times 1\ m^3$) under temperature- and humidity-controlled conditions (22–24 °C, 40–60% humidity) with a 12-h day-night cycle (lights on from 07:00 to 19:00). All dogs received food twice daily and had access to water *ad libitum*. To minimize individual variability, efforts were made to keep the life experiences of all animals as similar as possible. The behavioral experiment

(Experiment 1) was conducted on 28 adult male beagle dogs (14 wild type [WT] and 14 *Shank3* mutant dogs, Supplementary Table 1), each weighing between 10 and 16 kg. Of these, 12 dogs (6 WT and 6 *Shank3* mutants, Supplementary Table 1) were also involved in the electrophysiological experiment (Experiment 2). In the pharmacological rescue experiment (Experiment 3), 12 dogs (6 WT and 6 *Shank3* mutants) were assessed behaviorally, and 6 dogs (3 WT and 3 *Shank3* mutants) were also included in the electrophysiological assessment (Supplementary Table 1).

Nocifensive laser stimuli and behavioral assessment

Radiant-heat stimuli were generated using an infrared neodymium yttrium–aluminum perovskite (Nd:YAP) laser with a wavelength of 1.34 μm (Electronical Engineering, Italy). The laser pulse could selectively activate Aδ and C fiber nerve endings located in the superficial layers of the skin [41, 42]. The laser beam was transmitted through an optic fiber, and its diameter was set at ~7 mm on the target skin area by focusing lenses.

During the behavioral experiment, dogs were placed into a $0.6 \times 1.2 \times 1\ m^3$ box surrounded by transparent plastic boards, within which they could move freely. To test nocifensive sensitivity, graded laser pulses for 4 ms durations with ten stimulus intensities, ranging from 2.00–4.25 J with 0.25 J increments, were applied to the left forepaw of the dogs (Fig. 1A). Each dog was tested three times every other day (1 time/day), and in each test, ten stimuli with different intensities were delivered. The order of stimulus intensities was randomized, with an inter-stimulus interval of more than 1 min. The target site of the laser beam moved around to avoid repeatedly stimulating at the same spot [43]. After each stimulus, nocifensive behavior (i.e., forepaw withdrawal) was recorded by the experimenter, who was blinded to both the stimulus intensity and the dogs' genotype. No skin burn injuries were observed in each dog during all the tests. The nocifensive threshold was defined as the minimal stimulus intensity that elicited a left-forepaw withdrawal. Nocifensive behaviors were quantified by using a 0–3 numerical rating scale: 0, no movement; 1, flinching, i.e., small abrupt body jerking movement; 2, forepaw withdrawal gently, might accompanied by body tremble; 3, forepaw withdrawal with apparent avoidance behaviors, such as moving away from the laser beam.

Electrode implantation and electrophysiological recording

A 32-channel array of electrocorticographic (ECoG) recording electrodes (Kedounaoji, Jiangsu, China) was placed on the right brain hemisphere, following the method described previously [40, 44]. The reference and ground electrodes were both placed on the posterior occipital cortex. The location coordinates of the recording electrodes were determined using previously acquired magnetic resonance images and postoperative computed tomography images.

To systematically assess the dogs' neural responses to nociceptive stimuli, a session including five blocks of stimuli at different intensities was performed for each dog per day. Each block consisted of 30 stimuli with a fixed stimulus intensity delivered to the left forepaw of the dogs. Five low levels of stimulus intensity were used to prevent burns from repeated laser stimuli (I1–I5, 2.25–3.25 J with a 0.25 J increment, Fig. 1D). The sequence of stimulus intensities across blocks was randomized. The inter-stimulus interval was more than 30 s. To ensure the dogs' well-being and maintain their engagement, they received food rewards and were allowed to rest for at least 5 min between successive blocks with different stimulus intensities. The procedure was repeated five times for each dog, i.e., 5 sessions per dog and one session per day, which resulted in a total of 30 sessions for 6 WT and 6 *Shank3* mutant dogs, respectively (Supplementary Table 1).

ECoG recording and data analyses

ECoG data were amplified and recorded using the Zeus data acquisition system (Zeus, China; high pass: 0.01 Hz; sampling rate: 1000 Hz), and analyzed in MATLAB version 2020a (Mathworks Inc., Natick, MA) with the EEGLAB and FieldTrip toolboxes. Continuous ECoG data were band-pass filtered between 1 and 100 Hz, and notch filtered between 49 and 51 Hz to remove the 50-Hz powerline artifacts. Epochs were extracted using a 2000 ms analysis window (500 ms pre-stimulus and 1500 ms post-stimulus), and baseline-corrected using the pre-stimulus interval. Trials with amplitude exceeding ± 500 μV at any point across the time course for any electrode were considered to be contaminated by gross artifacts and were automatically rejected. Fewer than three trials were removed from each session for all dogs. Average LEP waveforms, time-locked to the onset of laser stimuli, were computed across all stimulus intensities for each dog (Fig. 1F).

Since radiant laser heat pulses concomitantly activate Aδ and C skin nociceptors, Aδ laser-evoked potentials (Aδ-LEPs) were observed to be followed by C-LEPs in humans [45]. Consistent with human findings, we observed two obvious negative-positive complexes in dog LEP responses, i.e., Aδ-N2/P2 complex occurring between 100 and 450 ms and C-N2/P2 complex occurring between 400 and 800 ms (Fig. 2C). Both responses were optimally detected from fronto-central electrodes with an average reference. Moreover, an early negative peak (Aδ-N1, occurring between 50 and 100 ms) preceding the Aδ-N2/P2 complex was clearly identified in LEP responses at post-central electrodes referenced to temporal electrodes, which showed a concurrent positive component. Baseline-to-peak amplitudes of the Aδ-N1 wave and peak-to-peak amplitudes of Aδ-N2/P2 and C-N2/P2 complexes were measured for each block in both groups. Brain topographies of these responses were computed using linear interpolation to reveal the spatial differences between WT and *Shank3* mutant dogs.

The time-frequency representations of LEP responses were calculated using a windowed Fourier transform with a fixed 300-ms Hanning window. This analysis yielded, for each trial, a complex spectral estimate $F(t, f)$ at each time-frequency point, extending from −500–1500 ms (in steps of 1 ms) in latency, and from 1–100 Hz (in steps of 0.5 Hz) in frequency. The spectrogram, $P(t, f)=|F(t, f)|^2$, represents the spectral power as a joint function of time and frequency at each time-frequency point [46]. Spectrograms were baseline-corrected by subtracting the average power within the pre-stimulus reference interval (−350−150 ms relative to stimulus onset) for each frequency. The reference interval was chosen to avoid the bias from windowing post-stimulus activity and padding values. The magnitudes of time-frequency features, including low-frequency LEP responses (LEP) and high-frequency gamma band oscillations (GBO), were extracted with specific time-frequency regions-of-interest (ROIs) [Aδ-LEP, 100–400 ms, 1–13 Hz; C-LEP: 400–800 ms, 1–13 Hz; Aδ-GBO, 100–400 ms, 60–95 Hz; C-GBO: 400–800 ms, 60–95 Hz] (Fig. 1F). These magnitudes were quantified by computing the top 20% of all time-frequency points within each ROI [47, 48].

A Fast Fourier Transformation was performed on each trial within the pre-stimulus time window ranging from –5–0 s to estimate the spectral power of resting-state brain oscillations [46]. This operation yielded a power spectrum ranging from 1–80 Hz, in steps of 2 Hz, for each electrode of each dog. Frequencies from 1–80 Hz were divided into five bands: delta (<4 Hz), theta (4–8 Hz), alpha (8–13 Hz), beta (13–30 Hz), and gamma (30–80 Hz). The total power within each frequency band was defined as the mean value of power spectra within the respective frequency range (Fig. 1F). Brain topographies of spectral powers of resting-state brain oscillations at these frequency bands were computed by linear interpolation. To extract the aperiodic exponent (Fig. 1F), we employed the FOOOF algorithm within the frequency range from 10–80 Hz [49]. The aperiodic exponent was calculated for each electrode, with a focus on fronto-central electrodes.

Pentylenetetrazole (PTZ) administration

PTZ, a $GABA_A$ receptor antagonist, increases the duration of the closed state of the $GABA_A$ receptor by inhibiting the GABA-activated Cl^- current in a concentration-dependent manner, thereby maintaining neuronal excitability [50]. To investigate whether the $GABA_A$ receptor antagonist could modulate the excitatory-inhibitory balance of neural activity in *Shank3* mutants and thus rescue abnormal nocifensive sensitivity (Experiment 3), we administered PTZ at a concentration of 1.5 mg/kg which could not induce seizures, as established in the previous study [40]. No seizures or other adverse effects were observed in dogs after PTZ administration. After saline or PTZ administration, the dogs were returned to their home cages for 30 min before performing experimental assays, which included nocifensive behavioral assessments and the collection of ECoG data.

Statistical analysis

All statistical analyses were carried out using the IBM SPSS 26 (IBM Corp., Armonk, NY) and R (version 4.0.2). Nocifensive threshold and resting-state ECoG features (i.e., spectral powers and the aperiodic exponent) were compared between *Shank3* mutant and WT dogs using the Mann-Whitney *U* test, with the common language effect size (*CLES*) quantifying the effect size. We compared cortical responses (i.e., time-domain LEP waves and time-frequency oscillations) evoked by nociceptive stimuli between *Shank3* mutant and WT dogs using mixed effect models implemented in the R package lme4 (ver 1.1–35.5).

To assess group differences in forepaw withdrawal behaviors and oscillatory responses across different stimulus intensities, two-way

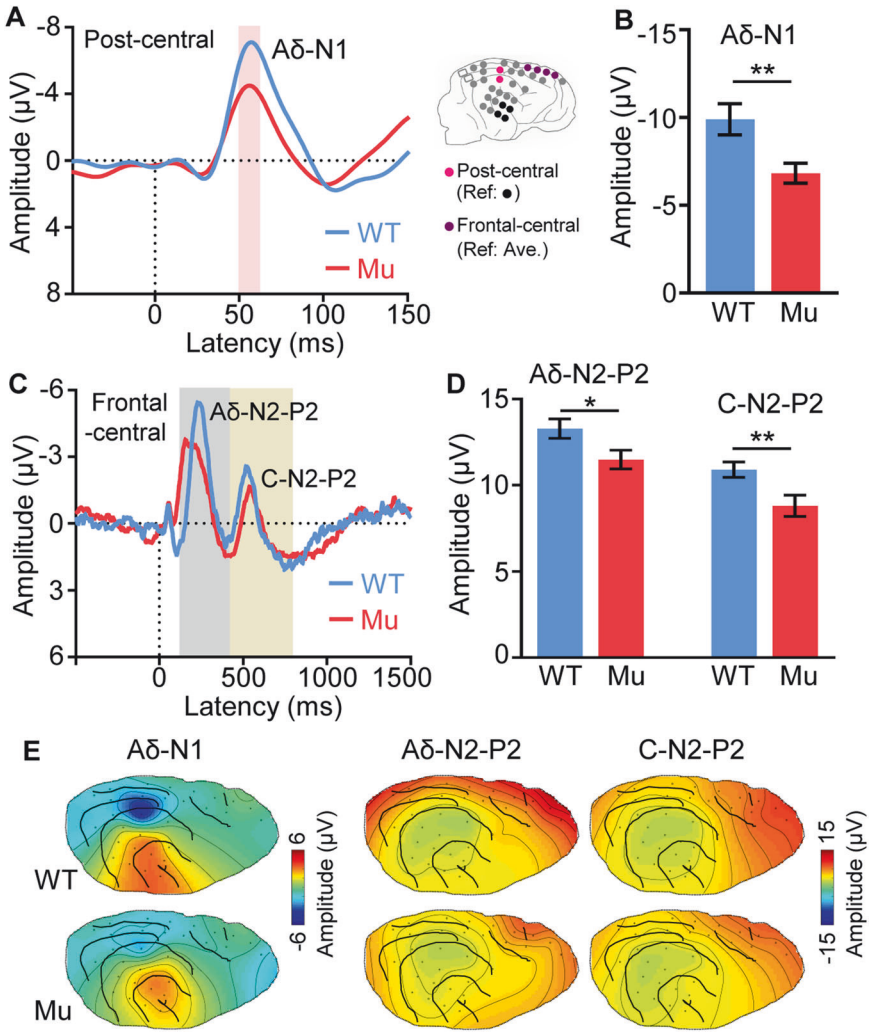

Fig. 2 Reduced cortical responses to nociceptive laser stimuli in *Shank3* mutant dogs. A Grand-averaged LEP responses recorded from the post-central cortex (pink electrodes), referenced to the temporal cortex (black electrodes), to extract the Aδ-N1 wave. **B** Comparison of Aδ-N1 amplitudes between WT and Mu dogs. **C** Grand-averaged LEP responses recorded from the fronto-central cortex (purple electrodes), referenced to the common average (Ave.), to extract the Aδ-N2/P2 and C-N2/P2 waves. **D** Comparison of the peak-to-peak amplitudes of Aδ-N2/P2 and C-N2/P2 waves between WT and Mu dogs. Data are represented as mean ± SEM. Statistical significance was determined using the mixed effect model, with $n = 150$ blocks per group. $^{*}p < 0.05$, $^{**}p < 0.01$. **E** Brain topographies of Aδ-N1 amplitudes and peak-to-peak amplitudes of Aδ-N2/P2 and C-N2/P2 waves in WT and *Shank3* mutant dogs.

repeated-measures analyses of variance (ANOVA) were performed, with stimulus intensity (I1–I5) as the within-subject factor and group (*Shank3* mutant and WT dogs) as a between-subject factor. Additionally, to assess the effects of PTZ on aperiodic exponents and nocifensive sensitivities, we used two-way repeated-measures ANOVA with condition (saline and PTZ administration) as the within-subject factor and group (*Shank3* mutant and WT dogs) as the between-subject factor. When significant main effects or interactions were identified, *post hoc* pairwise comparisons with Bonferroni correction were performed.

The relationships among nocifensive behaviors, cortical responses evoked by nociceptive stimuli, and pre-stimulus resting-state ECoG features were first assessed using correlation analyses. Bonferroni correction was applied to account for multiple comparisons. To reveal how the excitatory-inhibitory balance of the neural system, which is represented by the aperiodic exponent, influences the relationships between genotype (*Shank3* mutant and WT dogs) and nocifensive behaviors or cortical responses evoked by nociceptive stimuli, we built mediation models based on the correlation results following previous methods [51, 52]. The independent variable (X) in the model was the genotype, and the dependent variable (Y) was the forepaw withdrawal behavior in model 1 and cortical responses evoked by nociceptive stimuli in model 2. The aperiodic exponent, calculated from pre-stimulus ECoG data, was used as the mediator variable in both models. The mediation analyses were performed using AMOS 26.0 (SPSS Inc.), and the detailed procedures along with the criteria for the model fit were described in the previous studies [51, 52].

RESULTS

Reduced nocifensive sensitivity in *Shank3* mutant dogs

To evaluate whether the nocifensive reactivity was altered due to *Shank3* mutations, we assessed nocifensive sensitivity in *Shank3* mutant and WT dogs (Fig. 1A). We used a limited number ($n = 3$) of nociceptive stimuli at each intensity to elicit withdrawal behaviors of the dogs to minimize possible injuries to the subjects. We found that the nocifensive threshold in *Shank3* mutant dogs ($N = 14$, 3.71 ± 0.20 J) was significantly higher than WT dogs ($N = 14$, 2.40 ± 0.12 J, $Z = 16.50$, $p < 0.001$, $CLES = 0.940$; Fig. 1B). Nocifensive behavior scores, significantly increased with the increase of stimulus intensity ($F_{(9234)} = 28.202$, $p < 0.001$, $\eta^2 = 0.520$), were significantly higher in WT dogs than *Shank3* mutant dogs ($F_{(1,26)} = 14.88$, $p = 0.001$, $\eta^2 = 0.364$; Fig. 1C). There was no significant interaction between genotype and stimulus intensity ($F_{(9234)} = 1.378$, $p = 0.199$, $\eta^2 = 0.050$). These results

demonstrated that *Shank3* mutant dogs exhibit a reduced nocifensive sensitivity, regardless of stimulus intensity.

Reduced cortical responses to nociceptive stimuli in *Shank3* mutant dogs

To investigate whether neural responses elicited by nociceptive laser stimuli also altered due to *Shank3* mutations, we compared laser-evoked ECoG responses between *Shank3* mutant and WT dogs (Fig. 1D and E). Although with similar brain topographies (Fig. 2E), the amplitude of Aδ-N1 wave at about 60 ms after laser stimuli (i.e., maximal at post-central electrodes, likely generated from the primary somatosensory cortex, as suggested from human studies [45]) was significantly lower in *Shank3* mutant dogs than WT dogs (-6.83 ± 0.57 vs -9.90 ± 0.89 μV, $\chi^2 = 8.34$, $\beta = 3.069$, $t = 2.908$, $p = 0.004$; Fig. 2A, B). Similarly, peak-to-peak amplitudes of Aδ-N2/P2 and C-N2/P2 complexes, maximal at fronto-central electrodes (Fig. 2E) and likely originating from bilateral insula and anterior cingulate cortex [45], were significantly lower in *Shank3* mutant dogs than WT dogs (Aδ-N2/P2, 11.28 ± 0.54 vs 13.28 ± 0.56 μV, $\chi^2 = 5.60$, $\beta = -1.798$, $t = -2.377$, $p = 0.018$; C-N2/P2, 8.80 ± 0.62 vs 10.90 ± 0.45 μV, $\chi^2 = 7.59$, $\beta = -2.102$, $t = -2.773$, $p = 0.006$; Fig. 2C, D). Significant differences in Aδ-N2 and Aδ-P2 latencies between *Shank3* mutant and WT dogs were also observed (Supplementary Table 2). These results showed that *Shank3* mutants exhibit reduced cortical responses to nociceptive laser stimuli.

Time-frequency analysis revealed four distinct neural oscillatory responses to nociceptive laser stimuli in both *Shank3* mutant and WT dogs (Fig. 3A, B), including low-frequency (1–13 Hz) LEP responses (Aδ-LEP, 100–400 ms; C-LEP: 400–800 ms), and high-frequency (60–95 Hz) gamma-band oscillatory (GBO) responses (Aδ-GBO, 100–400 ms; C-GBO: 400–800 ms). Notably, brain topographies of all oscillatory responses were similarly maximal at fronto-central electrodes in both *Shank3* mutant and WT dogs (Fig. 3C). When compared with WT dogs, *Shank3* mutant dogs displayed significantly lower magnitudes of all oscillatory responses evoked by nociceptive laser stimuli (Aδ-LEP: 4.78 ± 0.33 vs 6.02 ± 0.48 μV²/Hz, $\chi^2 = 4.73$, $\beta = -1.240$, $t = -2.184$, $p = 0.030$; C-LEP: 3.77 ± 0.27 vs 5.05 ± 0.40 μV²/Hz, $\chi^2 = 6.91$, $\beta = -1.288$, $t = -2.644$, $p = 0.009$; Aδ-GBO: 0.10 ± 0.004 vs 0.15 ± 0.01 μV²/Hz, $\chi^2 = 22.52$, $\beta = -0.053$, $t = -4.837$, $p < 0.001$; C-GBO: 0.11 ± 0.005 vs 0.16 ± 0.008 μV²/Hz, $\chi^2 = 24.10$, $\beta = -0.048$, $t = -5.011$, $p < 0.001$; Fig. 3D, E). Additionally, these cortical responses exhibited consistent differences between *Shank3* mutant and WT dogs for most stimulus intensities, especially for gamma oscillations (Supplementary Fig. 1). Moreover, GBOs were dependent on nociceptive stimulus intensity (Aδ-GBO: $F_{(4232)} = 4.624$, $p = 0.001$, $\eta^2 = 0.074$; C-GBO: $F_{(4232)} = 10.104$, $p < 0.001$, $\eta^2 = 0.148$; Supplementary Tables 3 and 4) and significantly correlated with nocifensive sensitivity (Aδ-GBO: $r = -0.304$, $p < 0.001$; C-GBO: $r = -0.339$, $p < 0.001$; Supplementary Table 5).

Reduced powers of resting-state brain oscillations in *Shank3* mutant dogs

Previous studies demonstrated that brain oscillations during the resting state modulated the perception of nociceptive stimuli in humans [53]. To determine whether resting-state brain oscillations

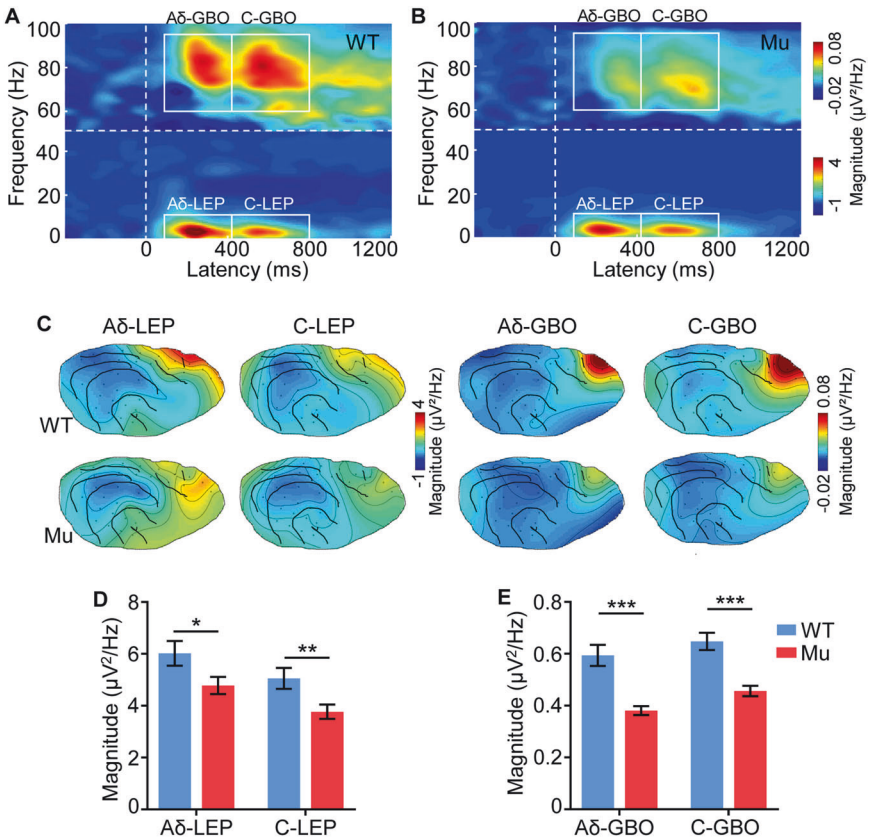

Fig. 3 Reduced oscillatory responses to nociceptive laser stimuli in *Shank3* mutant dogs. A, B Group-level time-frequency representations of laser-evoked cortical responses in the fronto-central cortex of WT and *Shank3* mutant dogs. The color scale represents the increase or decrease of oscillation magnitude relative to the pre-stimulus interval (−350−150 ms). Low-frequency LEP (1 Hz–13 Hz) and high-frequency GBO responses (60 Hz–95 Hz) are marked with white frames. **C** Brain topographies of Aδ-LEP, C-LEP, Aδ-GBO, and C-GBO in WT and *Shank3* mutant dogs. **D, E** Comparison of Aδ-LEP, C-LEP, Aδ-GBO, and C-GBO magnitudes between WT (blue) and *Shank3* mutant dogs (red). Statistical significance was determined using the mixed effect model, with $n = 150$ blocks per group. *$p < 0.05$, **$p < 0.01$, ***$p < 0.001$.

were also modulated by *Shank3* mutations, we compared the spectral powers of resting-state brain oscillations between WT and *Shank3* mutant dogs (Fig. 4A). Spectral power of resting-state brain oscillations in *Shank3* mutant dogs was significantly lower than in WT dogs at all frequency bands (delta: 14.74 ± 0.12 vs 15.31 ± 0.13 dB, $Z = -3.602$, $CLES = 0.819$; theta: 12.52 ± 0.10 vs 13.34 ± 0.12 dB, $Z = -5.199$, $CLES = 0.661$; alpha: 8.70 ± 0.13 vs 9.90 ± 0.11 dB, $Z = -8.497$, $CLES = 0.746$; beta: 5.12 ± 0.11 vs 8.19 ± 0.08 dB, $Z = -13.682$, $CLES = 0.970$; gamma: 1.01 ± 0.06 vs 4.12 ± 0.17 dB, $Z = -13.569$, $CLES = 0.952$; all $p < 0.001$; Fig. 4B), while brain topographies of spectral power within these frequency bands showed similar distributions between *Shank3* mutant and WT dogs (Fig. 4C).

Excitatory/inhibitory imbalance in *Shank3* mutant dogs

The aperiodic exponent, referred to as the slope of the aperiodic component of power spectra, has been used as a marker for the excitatory-inhibitory balance of neural activity [33, 35, 49] and is crucial for nociceptive processing [28–31]. To investigate whether the excitatory-inhibitory balance was altered due to *Shank3* mutations, we compared the aperiodic exponent in the mutant and WT dogs. Grand-averaged traces of aperiodic component of power spectra in *Shank3* mutant and WT dogs are shown in Fig. 5A. Although brain topographies of the aperiodic exponent were highly similar between *Shank3* mutant and WT dogs (Fig. 5B), *Shank3* mutants exhibited significantly lower aperiodic exponent than WT dogs (−1.26 ± 0.03 vs −1.13 ± 0.02, $Z = -3.903$, $p < 0.001$, $CLES = 0.616$; Fig. 5C). This result suggested that the excitatory-inhibitory balance of neural activity (i.e., E/I ratio) shifted to a more inhibited state due to *Shank3* mutations.

Correlation analyses revealed significant correlations between aperiodic exponent and (1) nocifensive sensitivity ($r = -0.239$, $p < 0.001$) and (2) laser-evoked neural oscillatory responses (Aδ-LEP: $r = 0.285$, $p < 0.001$; C-LEP: $r = 0.165$, $p = 0.004$; Aδ-GBO: $r = 0.235$, $p < 0.001$; C-GBO: $r = 0.221$, $p < 0.001$). Mediation models were built to assess the possible effect of aperiodic exponent on the relationship between genotype and nocifensive sensitivity or neural oscillatory responses. For the first mediation model (the dependent variable was the forepaw withdrawal upon nociceptive stimuli), genotype showed a direct (b = 0.954, SE = 0.006, CI = [0.939 0.964], $p = 0.010$) and indirect effect (b = 0.146, SE = 0.014, CI = [0.003, 0.026], $p = 0.016$) on nocifensive sensitivity through the aperiodic exponent (Fig. 5D). For the second mediation model (the dependent variable was cortical responses evoked by nociceptive stimuli), the aperiodic exponent also mediated the effect of genotype on cortical oscillatory responses, both directly (b = −0.250, SE = 0.078, CI = [−0.411 −0.106], $p = 0.015$) and indirectly (b = 0.030, SE = 0.018, CI = [0.001 0.068], $p = 0.031$; Fig. 5D). These results indicated that the aperiodic exponent, a marker of the E/I balance, mediated the relationship between genotype and nocifensive sensitivity as well as between genotype and neural oscillatory responses.

PTZ rescued altered E/I balance and nocifensive sensitivity in *Shank3* mutant dogs

It is well-established that $GABA_AR$ antagonists can enhance gamma oscillations [54] and increase neuronal excitability [50]. Therefore, we hypothesized that the $GABA_AR$ antagonist PTZ might modulate the E/I balance, thereby alleviating the reduced nocifensive sensitivity in *Shank3* mutants. As expected, PTZ increased the spectra of resting-state brain oscillations (Fig. 6B) and the slope of the aperiodic component of power spectra (Fig. 6C) in *Shank3* mutants. We also observed a significant interaction between groups (*Shank3* mutant and WT dogs) and conditions (saline and PTZ administration; $F_{(1133)} = 6.053$, $p = 0.015$, $\eta^2 = 0.044$). *Post hoc* pair-wise comparisons revealed that the aperiodic exponent was significantly modulated by PTZ in *Shank3* mutants (−1.37 ± 0.04 vs. −1.22 ± 0.05, $p = 0.015$) but not in WT controls (−0.99 ± 0.03 vs. −1.06 ± 0.06 μV, $p = 0.254$; Fig. 6D). This result suggests that the E/I balance of neural activity has shifted to a more activated state after PTZ administration in *Shank3* mutants. For nocifensive sensitivity, a significant main effect of condition was observed (saline vs. PTZ administration; $F_{(1,10)} = 18.617$, $p = 0.002$, $\eta^2 = 0.651$). *Post hoc* pair-wise comparisons revealed that *Shank3* mutant dogs exhibited increased nocifensive sensitivity after PTZ administration compared to saline administration ($N = 6$, 2.25 ± 0.13 J vs. 3.29 ± 0.36 J, $p = 0.020$). In contrast, no significant difference was observed between saline and PTZ administration in WT controls ($N = 6$, 2.54 ± 0.03 J vs. 2.13 ± 0.06 J, $p = 0.128$; Fig. 6A). Additionally, PTZ significantly

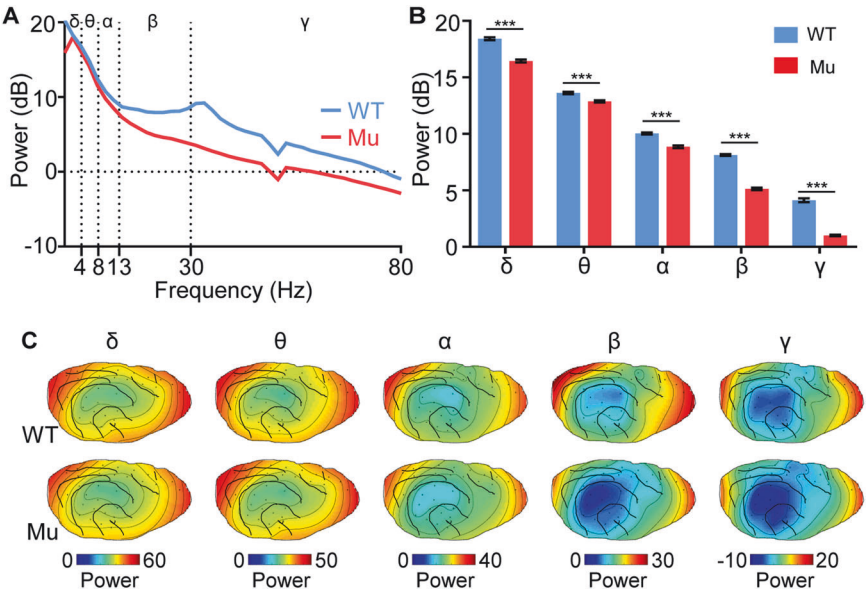

Fig. 4 Reduced spectral powers of resting-state brain oscillations in *Shank3* mutant dogs. A Group-level spectral powers of resting-state brain oscillations (averaged over 5 s pre-stimulus and across all electrodes) from *Shank3* mutant (red) and WT (blue) dogs. **B** Comparison of spectral powers at different frequency bands between the two groups. Statistical analysis was performed using the Mann-Whitney U test, with $n = 150$ blocks for each group. ***$p < 0.001$. **C** Brain topographies of spectral powers at different frequency bands in *Shank3* mutant and WT dogs.

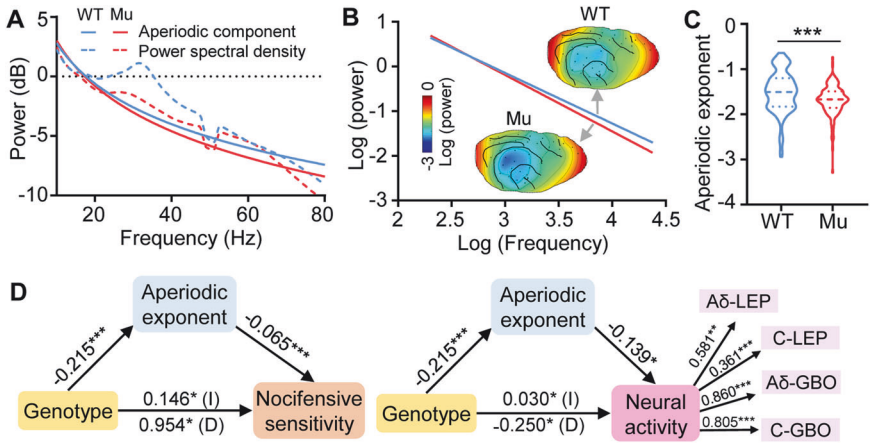

Fig. 5 The aperiodic exponent mediated the relationship between genotype and nocifensive sensitivity or neural responses evoked by nociceptive stimuli. A Group-level spectral power of resting-state brain oscillations, displaying both the overall spectral power (dashed lines) and the isolated aperiodic component (solid lines) for *Shank3* mutant (red) and WT (blue) dogs. **B** Group-level traces and brain topographies of the aperiodic component for *Shank3* mutant and WT dogs. **C** Comparison of aperiodic exponents from the fronto-central cortex between the two groups. Statistical analysis was performed using the Mann-Whitney U test, with $n = 150$ for each group. ***$p < 0.001$. **D** Mediation models illustrating how the aperiodic exponent mediated the effect of genotypes (*Shank3* mutant and WT dogs) on nocifensive sensitivity (left) and neural activities elicited by nociceptive laser stimuli (right). Standardized regression weights are shown in each model. D direct effect, I indirect effect. *$p < 0.05$, **$p < 0.01$, ***$p < 0.001$.

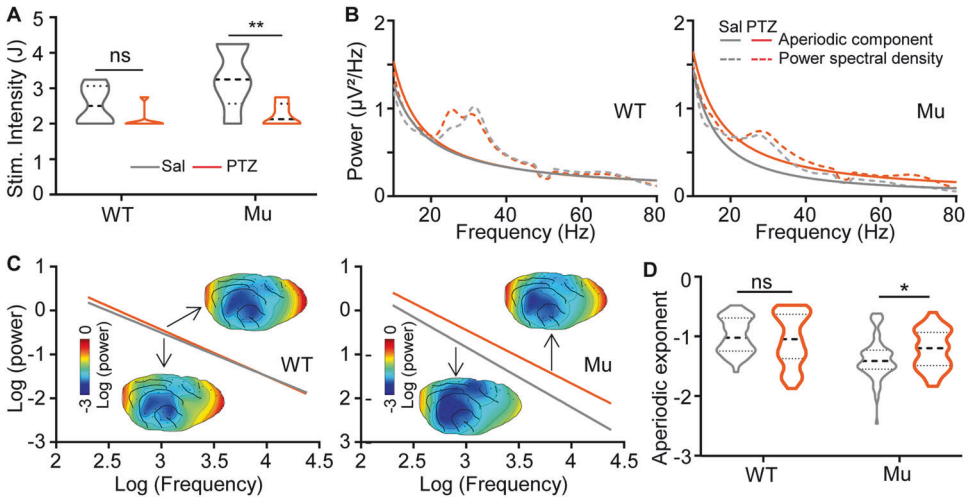

Fig. 6 PTZ improved nocifensive sensitivity and aperiodic exponent in *Shank3* mutants. A Comparison of nocifensive sensitivity between *Shank3* mutant ($N = 6$) and WT ($N = 6$) dogs after saline (grey) and PTZ (orange) administration. **B** Group-level power spectral density (dashed line) and its aperiodic component (solid line) of resting-state brain oscillations (150 s, 10 Hz–80 Hz) from *Shank3* mutant (right) and WT (left) dogs after saline (grey) and PTZ (orange) administration. **C** Group-level traces and brain topographies of aperiodic components for *Shank3* mutant (right) and WT (left) dogs after saline (grey) and PTZ (orange) administration. **D** Comparison of aperiodic exponents from the fronto-central cortex between *Shank3* mutant and WT dogs after saline (grey, $n = 90$ blocks) and PTZ (orange, $n = 45$ blocks) administration. ns: no significance, *$p < 0.05$, **$p < 0.01$.

increased nociceptive-evoked neural oscillations in *Shank3* mutant dogs, but not in WT controls (Supplementary Tables 6 and 7). These findings support the hypothesis that the E/I imbalance of neural activity underlies the impaired nocifensive reactivity in *Shank3* mutants.

DISCUSSION

In the present study, we observed reduced nocifensive reactivity —including both behavioral and electrophysiological responses— in a *Shank3* mutant dog model. The reduced nocifensive reactivity, characterized by decreases in behavioral sensitivity and Aδ-/C-LEP responses to nociceptive stimuli, recapitulates those observed in individuals with autism, including those with *SHANK3* mutations [12, 13] and *Shank3* mutant rodents [18, 55]. These findings thus reinforce the notion that reduced pain sensitivity is conserved characteristic of *SHANK3/Shank3*-related autism across species. Importantly, we demonstrated that impaired E/I balance of neural activity contributes to the reduced nocifensive reactivity in *Shank3* mutant dogs. Furthermore, adjusting the E/I imbalance towards a normal state by the $GABA_AR$ antagonist PTZ rescued the reduced nocifensive sensitivity in the mutants. Together, these findings for the first time revealed the critical role of E/I balance in pain processing associated with autism caused by *SHANK3/Shank3* mutations.

Laser pulses concomitantly activate Aδ- and C-fiber nociceptors, eliciting a typical double sensation in humans: an initial Aδ fiber-conducted pricking pain followed by a C fiber-conducted prolonged burning sensation because of the different conduction velocity of Aδ (~15 m/s) and C (~1 m/s) afferents [45]. The

concomitant activation of Aδ and C-nociceptors results in Aδ-LEP and C-LEP responses in the same trials [45, 56]. Different from humans, Aδ-fiber afferents in rodents are virtually insensitive to heat, meaning that the laser heat pulses only activate C-fiber afferents when delivered to the rat skin [57, 58]. In our study, the brain responses elicited by nociceptive laser stimuli in dogs showed clear deflections at latencies compatible with the conduction velocity of Aδ (Aδ-N1: ~60 ms, Aδ-N2/P2: 100–450 ms) and C fibers (C-N2/P2: 400–800 ms) (Fig. 2). The early N1 wave of the Aδ-LEPs may, as in human studies, originate from the primary somatosensory cortex and reflect somatosensory-specific activity correlated with the magnitude of the incoming nociceptive input [59, 60]. However, possibly due to the low-signal-to-noise ratio of C-N1 wave and the potential contamination from the preceding Aδ-N2/P2 complex, the N1 wave associated with the activation of C fibers was not identified in our study. Additionally, similar to our findings that both Aδ- and C-fiber LEP responses were significantly lower in *Shank3* mutant dogs compared to WT controls, autistic patients exhibit a significantly lower and prolonged P2-wave in response to nociceptive heat [6]. Autistic individuals show significantly lower responses to contact heat in typical pain-encoding brain regions, including the thalamus, S1, bilateral S2, insula, and dorsal anterior cingulate cortex [7], which are neural sources of Aδ-LEP and C-LEP responses. The similarity in cortical responses to nociceptive stimuli in both humans and dogs suggests that the reduced pain sensitivity associated with *SHANK3/Shank3* mutations may be evolutionarily conserved across species. These findings are unlikely to reflect temperament differences or attention deficits in mutants, as the changes in sensory sensitivity are different in different modalities (e.g., enhanced auditory sensitivity but reduced visual and tactile sensitivity) [40, 61].

Numerous studies suggest that cortical oscillations in the gamma frequency (i.e., GBOs) are one of the most promising neural markers of pain across species [47, 62–64]. GBOs could reliably correlate with pain perception intensity within individuals and pain sensitivity across different individuals, in both humans [47] and rodents [63]. GBO magnitude could also track the time-varying fluctuations of the intensity of pain [65–67]. Therefore, detecting GBOs in the *Shank3* mutant dog model would enable an objective and reliable examination of the dogs' nocifensive reactivity. Interestingly, time-frequency analysis in our study revealed the concomitant presence of two components of response corresponding to Aδ- and C-fiber responses, observed not only in the low-frequency range but also in the high-frequency gamma band (i.e., GBOs), which were also dependent on nociceptive stimulus intensities (Supplementary Tables 3 and 4). Moreover, we found that GBOs were significantly correlated with nocifensive sensitivity in dogs (Supplementary Table 5). *Shank3* mutant dogs exhibited significantly lower GBO magnitudes compared to WT dogs, which aligns with GBO abnormalities associated with various sensory processing in autistic individuals [68, 69]. These findings reinforce the notion that impaired nocifensive processing is presented in individuals with *SHANK3* mutations, and GBOs could be considered as a neural marker for diagnosing autism of abnormal nociceptive processing.

What are the potential neural mechanisms underlying reduced nocifensive reactivity in *Shank3* mutant dogs? The perceived intensity of a nociceptive stimulus is influenced by the state of brain immediately preceding the stimulus [53]. By examining resting-state brain oscillations, we found that spectral power was significantly lower in *Shank3* mutant dogs than WT dogs at all frequency bands (Fig. 4). This finding aligns with a report showing decreased spectral power across all frequency bands in the frontal regions of infants at high risk for autism [70]. Power spectra can be considered as a combination of aperiodic components and periodic oscillations [33, 49, 71]. Previous studies often overlook the impact of aperiodic signals on neural oscillations and extract the spectral power of brain oscillations without considering aperiodic activity [49]. This oversight may lead to inconsistent findings regarding spectral power across studies and could misinterpret results; for example, significant differences in spectral power across all frequency bands might stem solely from variations in the aperiodic component. Several studies have reported E/I imbalance (indicated by steeper slopes, as seen in Fig. 5) in various psychiatric disorders, including Rett Syndrome [72], Fragile-X syndrome [73], and Schizophrenia [74]. Other studies further report that the extent of E/I imbalance is correlated with the clinical severity of autistic phenotypes, such as social and sensory deficits [69, 75]. In the present study, *Shank3* mutant dogs showed that the E/I balance shifted toward inhibition. Additionally, mediation analyses revealed that reduced E/I ratios might underlie the impaired nocifensive reactivity in *Shank3* mutants. Furthermore, the $GABA_AR$ antagonist PTZ, increasing the duration of the excitatory state of neural activity [50], significantly shifted the abnormal E/I balance from inhibition to excitation, which was accompanied by increased nocifensive sensitivity in *Shank3* mutants. Thus, E/I balance in neural circuitry contributes, at least partially, to nocifensive reactivity in autism. *Shank3* encodes a post-synaptic scaffolding protein in excitatory synapses, and its loss results in impaired neural excitability and synaptic transmission in excitatory neurons [76]. We previously found reduced spontaneous excitatory postsynaptic currents while maintaining normal inhibitory postsynaptic currents in neuronal activity of pyramidal neurons due to *Shank3* mutations in dogs [77]. Thus, the reduced aperiodic exponent in *Shank3* mutant dogs could be attributed to a relatively enhanced inhibitory state arising from decreased excitatory synaptic transmission. Together with a previous report that the $GABA_AR$ antagonist PTZ ameliorated tactile and social impairments [40], our findings indicate that E/I balance might be a potential target for alleviating sensory and social deficits in autism.

Altogether, this study has provided mechanistic insights into abnormal pain processing in individuals with autism. However, a few limitations should be acknowledged. First, we used only transient nociceptive laser stimuli, leaving unclear how *Shank3* mutant dogs process sustained or different types of nociceptive stimuli (e.g., mechanical). Second, we examined changes of neural responses exclusively in the brain, leaving uncertain whether similar changes occur in the peripheral nervous system. Third, our study included adult dogs only, raising questions about the generalizability of these findings to younger ones. Fourth, although the average plasma half-life of the $GABA_AR$ antagonist PTZ was approximately 1.4 h in dogs [78], the duration of nociceptive modulation and potential side effects of PTZ remain unclear in dogs, warranting further investigation. Beyond targeting the GABA neurotransmitter, other neurotransmitters and their receptors [79, 80], such as dopamine, norepinephrine, and serotonin, may also serve as promising targets for rescuing nociceptive abnormalities associated with autism.

DATA AVAILABILITY

The data and analysis code that support the findings of this study are available from the corresponding authors upon reasonable request.

REFERENCES

1. Raja SN, Carr DB, Cohen M, Finnerup NB, Flor H, Gibson S, et al. The revised international association for the study of pain definition of pain: concepts, challenges, and compromises. Pain. 2020;161:1976–82.
2. Guan J, Li G. Injury mortality in individuals with autism. Am J Public Health. 2017;107:791–3.
3. Allely CS. Pain sensitivity and observer perception of pain in individuals with autistic spectrum disorder. ScientificWorldJournal. 2013;2013:e916178.
4. Moore DJ. Acute pain experience in individuals with autism spectrum disorders: a review. Autism. 2015;19:387–99.

5. Furniss F, Biswas AB. Recent research on aetiology, development and phenomenology of self-injurious behaviour in people with intellectual disabilities: a systematic review and implications for treatment. J Intellect Disabil Res. 2012;56:453–75.
6. Chien YL, Wu SW, Chu CP, Hsieh ST, Chao CC, Gau SSF. Attenuated contact heat-evoked potentials associated with sensory and social-emotional symptoms in individuals with autism spectrum disorder. Sci Rep. 2017;7:36887.
7. Failla MD, Moana-Filho EJ, Essick GK, Baranek GT, Rogers BP, Cascio CJ. Initially intact neural responses to pain in autism are diminished during sustained pain. Autism. 2018;22:669–83.
8. Rubinstein M, Patowary A, Stanaway IB, McCord E, Nesbitt RR, Archer M, et al. Association of rare missense variants in the second intracellular loop of NaV1.7 sodium channels with familial autism. Mol Psychiatry. 2018;23:231–9.
9. Oberman LM, Boccuto L, Cascio L, Sarasua S, Kaufmann WE. Autism spectrum disorder in Phelan-McDermid syndrome: initial characterization and genotype-phenotype correlations. Orphanet J Rare Dis. 2015;10:105.
10. Yuan B, Wang M, Wu X, Cheng P, Zhang R, Zhang R, et al. Identification of de novo mutations in the chinese autism spectrum disorder cohort via whole-exome sequencing unveils brain regions implicated in autism. Neurosci Bull. 2023;39:1469–80.
11. Monteiro P, Feng G. SHANK proteins: roles at the synapse and in autism spectrum disorder. Nat Rev Neurosci. 2017;18:147–57.
12. Sarasua SM, Boccuto L, Sharp JL, Dwivedi A, Chen C-F, Rollins JD, et al. Clinical and genomic evaluation of 201 patients with Phelan–McDermid syndrome. Hum Genet. 2014;133:847–59.
13. Tavassoli T, Layton C, Levy T, Rowe M, George-Jones J, Zweifach J, et al. Sensory reactivity phenotype in Phelan-Mcdermid syndrome is distinct from idiopathic ASD. Genes. 2021;12:977.
14. Ko HG, Oh SB, Zhuo M, Kaang BK. Reduced acute nociception and chronic pain in Shank2-/- mice. Mol Pain. 2016;12:1744806916647056.
15. Price TJ, Rashid MH, Millecamps M, Sanoja R, Entrena JM, Cervero F. Decreased nociceptive sensitization in mice lacking the fragile X mental retardation protein: role of mGluR1/5 and mTOR. J Neurosci. 2007;27:13958–67.
16. Wang L, Almeida LEF, Nettleton M, Khaibullina A, Albani S, Kamimura S, et al. Altered nocifensive behavior in animal models of autism spectrum disorder: the role of the nicotinic cholinergic system. Neuropharmacology. 2016;111:323–34.
17. Chen Y, Yu J, Niu Y, Qin D, Liu H, Li G, et al. Modeling rett syndrome using TALEN-edited MECP2 mutant cynomolgus monkeys. Cell. 2017;169:945–55.
18. Han Q, Kim YH, Wang X, Liu D, Zhang ZJ, Bey AL, et al. SHANK3 deficiency impairs heat hyperalgesia and TRPV1 signaling in primary sensory neurons. Neuron. 2016;92:1279–93.
19. Bunford N, Andics A, Kis A, Miklósi Á, Gácsi M. *Canis familiaris* as a model for non-invasive comparative neuroscience. Trends Neurosci. 2017;40:438–52.
20. Topál J, Román V, Turcsán B. The dog (*Canis familiaris*) as a translational model of autism: it is high time we move from promise to reality. Wiley Interdiscip Rev Cogn Sci. 2019;10:e1495.
21. Czeibert K, Andics A, Petneházy Ö, Kubinyi E. A detailed canine brain label map for neuroimaging analysis. Biol Futur. 2019;70:112–20.
22. Hernandez-Avalos I, Mota-Rojas D, Mora-Medina P, Martínez-Burnes J, Casas Alvarado A, Verduzco-Mendoza A, et al. Review of different methods used for clinical recognition and assessment of pain in dogs and cats. Int J Vet Sci Med. 2019;7:43–54.
23. van Oostrom H, Stienen PJ, Doornenbal A, Hellebrekers LJ. Nociception-related somatosensory evoked potentials in awake dogs recorded after intra epidermal electrical stimulation. Eur J Pain. 2009;13:154–60.
24. Rutherford KMD. Assessing pain in animals. Anim Welf. 2002;11:31–53.
25. Barry RJ, De Blasio FM. Characterizing pink and white noise in the human electroencephalogram. J Neural Eng. 2021;18:034001.
26. Donoghue T, Watrous AJ. How can we differentiate narrow-band oscillations from aperiodic activity? Intracranial EEG: A Guide for Cognitive Neuroscientists. Cham: Springer International Publishing; 2023. p. 351–64.
27. Ahmad J, Ellis C, Leech R, Voytek B, Garces P, Jones E, et al. From mechanisms to markers: novel noninvasive EEG proxy markers of the neural excitation and inhibition system in humans. Transl Psychiatry. 2022;12:467.
28. Peirs C, Seal RP. Neural circuits for pain: recent advances and current views. Science. 2016;354:578–84.
29. Torsney C, MacDermott AB. Disinhibition opens the gate to pathological pain signaling in superficial neurokinin 1 receptor-expressing neurons in rat spinal cord. J Neurosci. 2006;26:1833–43.
30. Xiong W, Ping X, Ripsch MS, Chavez GSC, Hannon HE, Jiang K, et al. Enhancing excitatory activity of somatosensory cortex alleviates neuropathic pain through regulating homeostatic plasticity. Sci Rep. 2017;7:12743.
31. Han Q, Wang H, Lu X, Li Y, Guo Y, Zhao X, et al. Preoperative resting-state electrophysiological signals predict acute but not chronic postoperative pain. Eur J Pain. 2025;29:e4757.
32. Chini M, Pfeffer T, Hanganu-Opatz I. An increase of inhibition drives the developmental decorrelation of neural activity. eLife. 2022;11:e78811.
33. Gao R, Peterson EJ, Voytek B. Inferring synaptic excitation/inhibition balance from field potentials. Neuroimage. 2017;158:70–78.
34. Lombardi F, Herrmann HJ, de Arcangelis L. Balance of excitation and inhibition determines 1/f power spectrum in neuronal networks. Chaos. 2017;27:047402.
35. Lendner JD, Helfrich RF, Mander BA, Romundstad L, Lin JJ, Walker MP, et al. An electrophysiological marker of arousal level in humans. eLife. 2020;9:e55092.
36. Gonzalez-Burgos I, Bainier M, Gross S, Schoenenberger P, Ochoa JA, Valencia M, et al. Glutamatergic and GABAergic receptor modulation present unique electrophysiological fingerprints in a concentration-dependent and region-specific manner. eNeuro. 2023;10:ENEURO.0406-22.2023.
37. Potter LE, Paylor JW, Suh JS, Tenorio G, Caliaperumal J, Colbourne F, et al. Altered excitatory-inhibitory balance within somatosensory cortex is associated with enhanced plasticity and pain sensitivity in a mouse model of multiple sclerosis. J Neuroinflammation. 2016;13:142.
38. Tian R, Li Y, Zhao H, Lyu W, Zhao J, Wang X, et al. Modeling Shank3-associated autism spectrum disorder in beagle dogs via CRISPR/Cas9 gene editing. Mol Psychiatry. 2023;28:3739–50.
39. Ren W, Yu S, Guo K, Lu C, Zhang YQ. Disrupted human-dog interbrain neural coupling in autism-associated Shank3 mutant dogs. Adv Sci. 2024;11:e2402493.
40. Shi Q, Wu L, Ren B, Guo K, Jiang Y-H, Zhang YQ, et al. Impaired tactile processing in autism-associated Shank3 mutant dogs: neural mechanism and intervention. Sci Bull. 2025;70:483–7.
41. Bromm B, Treede RD. Laser-evoked cerebral potentials in the assessment of cutaneous pain sensitivity in normal subjects and patients. Rev Neurol. 1991;147:625–43.
42. Carmon A, Mor J, Goldberg J. Evoked cerebral responses to noxious thermal stimuli in humans. Exp Brain Res. 1976;25:103–7.
43. Leandri M, Saturno M, Spadavecchia L, Iannetti GD, Cruccu G, Truini A. Measurement of skin temperature after infrared laser stimulation. Neurophysiol Clin. 2006;36:207–18.
44. Wu L, Mei S, Yu S, Han S, Zhang YQ. Shank3 mutations enhance early neural responses to deviant tones in dogs. Cereb Cortex. 2023;33:10546–57.
45. Hu L, Cai MM, Xiao P, Luo F, Iannetti GD. Human brain responses to concomitant stimulation of Aδ and C nociceptors. J Neurosci. 2014;34:11439–51.
46. Hu L, Zhang Z. EEG signal processing and feature extraction. Singapore: Springer Singapore; 2019.
47. Hu L, Iannetti GD. Neural indicators of perceptual variability of pain across species. Proc Natl Acad Sci USA. 2019;116:1782–91.
48. Mitsis GD, Iannetti GD, Smart TS, Tracey I, Wise RG. Regions of interest analysis in pharmacological fMRI: How do the definition criteria influence the inferred result? Neuroimage. 2008;40:121–32.
49. Donoghue T, Haller M, Peterson EJ, Varma P, Sebastian P, Gao R, et al. Parameterizing neural power spectra into periodic and aperiodic components. Nat Neurosci. 2020;23:1655–65.
50. Huang RQ, Bell-Horner CL, Dibas MI, Covey DF, Drewe JA, Dillon GH. Pentylenetetrazole-Induced inhibition of recombinant γ-Aminobutyric acid Type A (GABAA) receptors: mechanism and site of action. J Pharmacol Exp Ther. 2001;298:986–95.
51. Wu X, Lu X, Zhang H, Bi Y, Gu R, Kong Y, et al. Sex difference in trait empathy is encoded in the human anterior insula. Cereb Cortex. 2023;33:5055–65.
52. Zhang H, Bi Y, Hou X, Lu X, Tu Y, Hu L. The role of negative emotions in sex differences in pain sensitivity. Neuroimage. 2021;245:118685.
53. Tu Y, Zhang Z, Tan A, Peng W, Hung YS, Moayedi M, et al. Alpha and gamma oscillation amplitudes synergistically predict the perception of forthcoming nociceptive stimuli. Hum Brain Mapp. 2016;37:501–14.
54. Yamazaki M, Honda S, Tamaki K, Irie M, Mihara T. Effects of (+)-bicuculline, a GABAa receptor antagonist, on auditory steady state response in free-moving rats. PLoS ONE. 2020;15:e0236363.
55. Song TJ, Lan XY, Wei MP, Zhai FJ, Boeckers TM, Wang JN, et al. Altered behaviors and impaired synaptic function in a novel rat model with a complete Shank3 deletion. Front Cell Neurosci. 2019;13:111.
56. Jin QQ, Wu GQ, Peng WW, Xia XL, Hu L, Iannetti GD. Somatotopic representation of second pain in the primary somatosensory cortex of humans and rodents. J Neurosci. 2018;38:5538–50.
57. Hu L, Xia XL, Peng WW, Su WX, Luo F, Yuan H, et al. Was it a pain or a sound? across-species variability in sensory sensitivity. Pain. 2015;156:2449.
58. Xia XL, Peng WW, Iannetti GD, Hu L. Laser-evoked cortical responses in freely-moving rats reflect the activation of C-fibre afferent pathways. Neuroimage. 2016;128:209–17.
59. Lee MC, Mouraux A, Iannetti GD. Characterizing the cortical activity through which pain emerges from nociception. J Neurosci. 2009;29:7909–16.
60. Valentini E, Hu L, Chakrabarti B, Hu Y, Aglioti SM, Iannetti GD. The primary somatosensory cortex largely contributes to the early part of the cortical response elicited by nociceptive stimuli. Neuroimage. 2012;59:1571–81.

61. Ren W, Huang K, Li Y, Yang Q, Wang L, Guo K, et al. Altered pupil responses to social and non-social stimuli in Shank3 mutant dogs. Mol Psychiatry. 2023;28:3751–9.
62. Gross J, Schnitzler A, Timmermann L, Ploner M. Gamma oscillations in human primary somatosensory cortex reflect pain perception. PLoS Biol. 2007;5:e133.
63. Peng W, Xia X, Yi M, Huang G, Zhang Z, Iannetti G, et al. Brain oscillations reflecting pain-related behavior in freely moving rats. Pain. 2018;159:106–18.
64. Zhang LB, Chen YX, Li ZJ, Geng XY, Zhao XY, Zhang FR, et al. Advances and challenges in neuroimaging-based pain biomarkers. Cell Rep Med. 2024;5:101784.
65. Schulz E, Tiemann L, Witkovsky V, Schmidt P, Ploner M. Gamma oscillations are involved in the sensorimotor transformation of pain. J Neurophysiol. 2012;108:1025–31.
66. Li Z, Zhang L, Zeng Y, Zhao Q, Hu L. Gamma-band oscillations of pain and nociception: a systematic review and meta-analysis of human and rodent studies. Neurosci Biobehav Rev. 2023;146:105062.
67. May ES, Nickel MM, Ta Dinh S, Tiemann L, Heitmann H, Voth I, et al. Prefrontal gamma oscillations reflect ongoing pain intensity in chronic back pain patients. Hum Brain Mapp. 2019;40:293–305.
68. Rojas DC, Wilson LB. γ-band abnormalities as markers of autism spectrum disorders. Biomark Med. 2014;8:353–68.
69. Simon DM, Wallace MT. Dysfunction of sensory oscillations in autism spectrum disorder. Neurosci Biobehav Rev. 2016;68:848–61.
70. Tierney AL, Gabard-Durnam L, Vogel-Farley V, Tager-Flusberg H, Nelson CA. Developmental trajectories of resting EEG power: an endophenotype of autism spectrum disorder. PLoS ONE. 2012;7:e39127–e39127.
71. Buzsáki G, Logothetis N, Singer W. Scaling brain size, keeping timing: evolutionary preservation of brain rhythms. Neuron. 2013;80:751–64.
72. Roche KJ, LeBlanc JJ, Levin AR, O'Leary HM, Baczewski LM, Nelson CA. Electroencephalographic spectral power as a marker of cortical function and disease severity in girls with Rett syndrome. J Neurodev Disord. 2019;11:15.
73. Wilkinson CL, Nelson CA. Increased aperiodic gamma power in young boys with fragile X syndrome is associated with better language ability. Mol Autism. 2021;12:17.
74. Molina JL, Voytek B, Thomas ML, Joshi YB, Bhakta SG, Talledo JA, et al. Memantine effects on electroencephalographic measures of putative excitatory/inhibitory balance in schizophrenia. Biol Psychiatry Cogn Neurosci Neuroimaging. 2020;5:562–8.
75. Foss-Feig JH, Adkinson BD, Ji JL, Yang G, Srihari VH, McPartland JC, et al. Searching for cross-diagnostic convergence: neural mechanisms governing excitation and inhibition balance in schizophrenia and autism spectrum disorders. Biol Psychiatry. 2017;81:848–61.
76. Jiang YH, Ehlers MD. Modeling autism by SHANK gene mutations in mice. Neuron. 2013;78:8–27.
77. Zhu F, Shi Q, Jiang Y, Zhang YQ, Zhao H. Impaired synaptic function and hyperexcitability of the pyramidal neurons in the prefrontal cortex of autism-associated Shank3 mutant dogs. Mol Autism. 2024;15:9.
78. Jun HW. Pharmacokinetic studies of pentylenetetrazol in dogs. J Pharm Sci. 1976;65:1038–41.
79. Kirkpatrick DR, McEntire DM, Hambsch ZJ, Kerfeld MJ, Smith TA, Reisbig MD, et al. Therapeutic basis of clinical pain modulation. Clin Transl Sci. 2015;8:848–56.
80. Cetin FH, Tunca H, Güney E, Iseri E. Neurotransmitter systems in autism spectrum disorder. In: Fitzgerald M (ed). Autism Spectrum Disorder-Recent Advances. InTech: London. 2015, pp 15–30.

ACKNOWLEDGEMENTS

We thank Professor K. Guo and members of the Zhang laboratory for discussion. This work was supported in part by grants from the National Key Research and Development Program (2021ZD0203901 to Y.Z.), the National Science Foundation of China (32394030 to Y.Z., 32071061 to L.H.), the Beijing Natural Science Foundation (JQ22018 to L.H.), Wuhan Municipal S&T Project (Grant No. 2024020702030125 to Y.Z.), and sample storage by the Canine Biobank, Chinese Academy of Sciences (KFJ-BRP-004 to Y.Z.).

AUTHOR CONTRIBUTIONS

Conceptualization: QS, LH, YZ; Methodology: QS, LH; Software: QS, LH; Validation: QS; Formal analysis: QS; Investigation: QS, BR, LW; Resources: LH, YZ; Data curation: QS; Writing – original draft preparation: QS, LH, YZ; Writing – review & editing: XL, LZ, YZ, LH; Visualisation: QS; Supervision: LH, YZ; Project administration: LH, YZ; Funding acquisition: LH, YZ.

COMPETING INTERESTS

The authors declare no competing interests.

ADDITIONAL INFORMATION

Supplementary information The online version contains supplementary material available at https://doi.org/10.1038/s41380-025-02952-y.

Correspondence and requests for materials should be addressed to Li Hu or Yong Q. Zhang.